The Astrophysical Journal, 637:727–740, 2006 February 1
© 2006. The American Astronomical Society. All rights reserved. Printed in U.S.A.

LINKING STELLAR MASS AND STAR FORMATION IN *SPITZER* MIPS 24 μm GALAXIES

K. I. Caputi,[1] H. Dole,[1] G. Lagache,[1] R. J. McLure,[2] J-L. Puget,[1] G. H. Rieke,[3] J. S. Dunlop,[2]
E. Le Floc'h,[3] C. Papovich,[3,4] and P. G. Pérez-González[3]
Received 2005 June 7; accepted 2005 October 3

ABSTRACT

We present deep $K_s < 21.5$ (Vega) identifications, redshifts, and stellar masses for most of the sources composing the bulk of the 24 μm background in the GOODS/CDFS. Our identified sample consists of 747 *Spitzer* MIPS 24 μm objects and includes $\sim$94% of all the 24 μm sources in the GOODS-South field that have fluxes $S_\nu(24\ \mu\mathrm{m}) > 83\ \mu$Jy (the $\sim$80% completeness limit of the *Spitzer*/GTO 24 μm catalog); 36% of our galaxies have spectroscopic redshifts (mostly at $z < 1.5$), and the remaining ones have photometric redshifts of very good quality, with a median of $|dz| = |z_{\mathrm{spec}} - z_{\mathrm{phot}}|/(1 + z_{\mathrm{spec}}) = 0.02$. We find that MIPS 24 μm galaxies span the redshift range $z \sim 0$–4 and that a substantial fraction (28%) lie at high redshifts $z \gtrsim 1.5$. We determine the existence of a bump in the redshift distribution at $z \sim 1.9$, indicating the presence of a significant population of galaxies with PAH emission at these redshifts. The 24 μm galaxy population ranges from sources with intermediate luminosities ($10^{10}\ L_\odot < L_{\mathrm{IR}} < 10^{11}\ L_\odot$) and low-to-intermediate assembled stellar masses ($10^9\ M_\odot \lesssim M \lesssim 10^{11}\ M_\odot$) at $z \lesssim 0.8$, to massive ($M \gtrsim 10^{11}\ M_\odot$) hyperluminous galaxies ($L_{\mathrm{IR}} > 10^{12}\ L_\odot$) at redshifts $z \sim 2$–3. Massive star-forming galaxies at redshifts $2 \lesssim z \lesssim 3$ are characterized by very high star formation rates (SFR $> 500\ M_\odot\ \mathrm{yr}^{-1}$), and some of them are able to construct a mass of $\approx 10^{10}$–$10^{11}\ M_\odot$ in a single burst lifetime ($\sim$0.01–0.1 Gyr). At lower redshifts $z \lesssim 2$, massive star-forming galaxies are also present but appear to be building their stars on long timescales, either quiescently or in multiple modest burstlike episodes. At redshifts $z \sim 1$–2, the ability of the burstlike mode to produce entire galaxies in a single event is limited to some lower ($M \lesssim 7 \times 10^{10}\ M_\odot$) mass systems, and it is basically negligible at $z \lesssim 1$. Our results support a scenario in which star formation activity is differential with assembled stellar mass and redshift, and where the relative importance of the burstlike mode proceeds in a downsizing way from high to low redshifts.

Subject headings: galaxies: evolution — galaxies: statistics — infrared: galaxies

1. INTRODUCTION

Infrared (IR) surveys provide an unbiased way of studying the star formation history of the universe. The *Spitzer Space Telescope* (Werner et al. 2004), with its unprecedented sensitivity, is revolutionizing our understanding of IR galaxy evolution by obtaining very deep IR maps. The previous space IR facilities, the *Infrared Astronomical Satellite* (*IRAS*) and the *Infrared Space Observatory* (*ISO*), set the first constraints on mid- and far-IR galaxy evolution at $z \lesssim 1$ (see Genzel & Cesarsky [2000] and Franceschini et al. [2001] for a review). Deep *Spitzer* images offer the possibility of exploring star formation in the high-redshift universe, covering the gap between *ISO* sources and the still limited quantity of known submillimeter sources at redshifts $z \sim 2$–3 (e.g., Scott et al. 2002; Borys et al. 2003; Chapman et al. 2003).

The study of IR sources at high redshifts is useful to put constraints on the early stages of star and galaxy formation. An important cosmological issue is the determination of what kind of galaxies host star formation activity at different redshifts. At $z \sim 1$, a mixture of star-forming objects is found, from massive spiral galaxies to ongoing starbursts (Franceschini et al. 2003; Bell et al. 2005). In addition, it is known that star formation can proceed on different timescales, from bursts produced in short time periods (typically 0.01–0.1 Gyr) to sources with extended periods of quiescent activity. The study of the evolution of the full range of star-forming galaxies should allow reconstruction of the star formation history of the universe.

Several empirical approaches based on *IRAS*/*ISO* surveys have predicted the existence of a substantial population of mid-IR galaxies at high redshifts. Very recently, based on the modeling of the number counts of *Spitzer* 24 μm galaxies, Lagache et al. (2004) concluded that the polycyclic aromatic hydrocarbon (PAH) emission characteristic of the interstellar medium (Désert et al. 1990) should remain observable in galaxies up to $z \sim 2.5$. The main PAH spectral features are located at rest-frame wavelengths $\lambda_{\mathrm{rf}} = 3.3$, 6.2, 7.7, 8.6, 11.3, 12.7, 16.3, and 17 μm. If present, these emission lines should enter the 24 μm filter at redshifts $z \sim 6.3$, 2.9, 2.1, 1.8, 1.1, 0.9, 0.5, and 0.4, respectively. Thus, if PAH molecules already exist in high-redshift galaxies, they should appear in the 24 μm passband, producing the selection of a substantial population of sources at redshifts $z \gtrsim 1$ (Papovich et al. 2004).

In this work we present K_s-band identifications, redshifts, and stellar mass estimates for most of the sources composing the 24 μm background down to faint fluxes in $\sim$131 arcmin^2 of the Great Observatories Origins Deep Survey Chandra Deep Field–South (GOODS/CDFS), achieving 94% identification completeness for sources with flux $S_\nu(24\ \mu\mathrm{m}) > 83\ \mu$Jy. The mostly complete redshift identification of *Spitzer* 24 μm sources with magnitudes $R < 24$ (Vega) at $z \lesssim 1$ has already been achieved by Le Floc'h et al. (2005) over an extended area of the CDFS. Evidence of luminous infrared galaxies up to redshift $z \sim 2.5$ has been reported by different authors (Le Floc'h et al. 2004; Lonsdale et al. 2004; Papovich et al. 2006). The evolution of the mid-IR luminosity function and the derived SFR densities have been explored by Le Floc'h et al. (2005) and Pérez González et al. (2005). The present work, albeit based on the

[1] Institut d'Astrophysique Spatiale, Bâtiment 121, Université Paris Sud, F-91405 Orsay Cedex, France.
[2] Institute for Astronomy, University of Edinburgh, Royal Observatory, Blackford Hill, Edinburgh EH9 3HJ, UK.
[3] Steward Observatory, University of Arizona, 933 North Cherry Avenue, Tucson, AZ 85721.
[4] Spitzer Fellow.

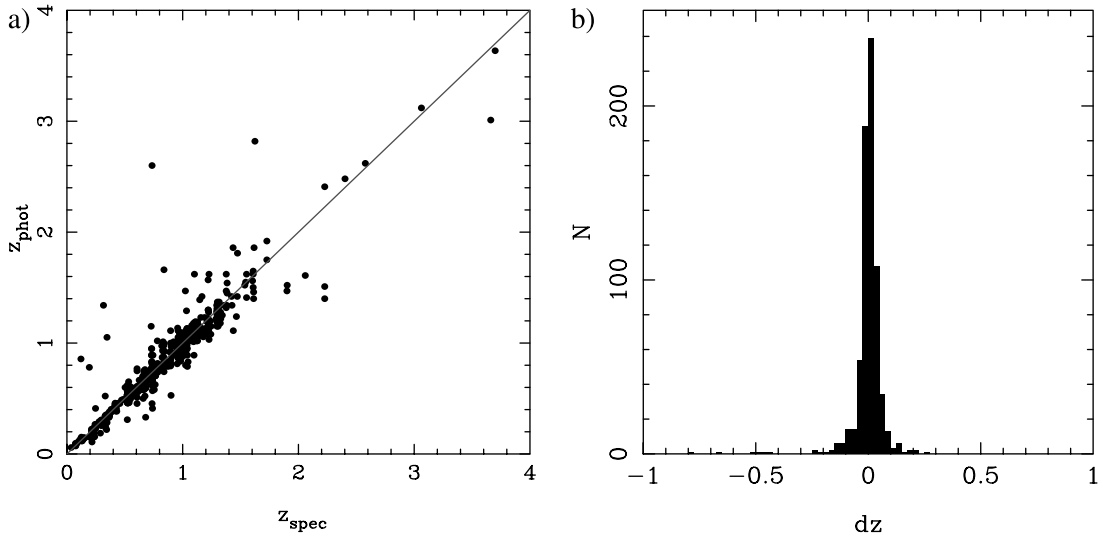


FIG. 1.—(*a*) Photometric vs. spectroscopic redshifts for $K_s < 21.5$ galaxies in the GOODS/CDFS. (*b*) Histogram of the relative errors $dz = (z_{spec} - z_{phot})/(1 + z_{spec})$. The rms of this distribution is 0.03.

study of a smaller area, complements the former, as it exploits the unique quality of the GOODS data sets to obtain an almost complete identification of the sources composing the mid-IR background and to characterize some of their most important properties from low to high redshifts (from $z \approx 0$ to $z \approx 3$–4).

The organization of this paper is as follows. In § 2 we summarize the data sets and catalogs used to construct the source sample analyzed in the present study. In § 3 we present the redshift distribution of the 24 μm galaxy population in the GOODS/CDFS. In § 4 we give estimates of their characteristic stellar masses. In § 5 we study the evolution of IR luminosities and stellar masses with redshift and put constraints on the SFRs and timescales for star formation activity in different mass galaxies. Finally, in § 6 we summarize our results and present some concluding remarks. We adopt throughout a cosmology with $H_0 = 70$ km s^{-1} Mpc^{-1}, $\Omega_M = 0.3$, and $\Omega_\Lambda = 0.7$.

2. K_s-BAND COUNTERPARTS TO MIPS 24 μm SOURCES

2.1. *The Data Samples and Redshift Estimates*

Deep 24 μm observations of $\sim$2000 arcmin^2 of the CDFS have been carried out with the Multiband Imaging Photometer for *Spitzer* (MIPS; Rieke et al. 2004), as part of the Guaranteed Time Observers (GTO) program. The data reduction, extraction of sources, and photometry measurements are explained in detail in Papovich et al. (2004). The source catalog achieves 80% completeness at a flux limit of $S_\nu \sim 83$ μJy, and the fraction of spurious sources at that limit is determined to be <10%. The 24 μm source density in the CDFS is $N(S_\nu > 83\ \mu\text{Jy}) = 4.5$ arcmin^{-2}. Above a flux of $S_\nu \sim 60$ μJy, resolved *Spitzer* sources account for $\sim$70% of the 24 μm cosmic infrared background (Papovich et al. 2004; Lagache et al. 2004).

The GOODS project (Giavalisco et al. 2004) has provided deep multiwavelength data for $\sim$160 arcmin^2 of the CDFS. The data products are released to the astronomical community in a fully reduced mode. As part of the European Southern Observatory GOODS Imaging Survey program (ESO GOODS/EIS; B. Vandame et al. 2006, in preparation), deep *J*- and K_s-band images taken with the Infrared Spectrometer and Array Camera (ISAAC) on the Very Large Telescope (VLT) have been made public for $\sim$131 arcmin^2 of the GOODS/CDFS. This is the area analyzed in the present work. The ESO/EIS imaging in this field is complemented by deep imaging data in the *B*, *V*, I_{775}, and z_{850} bands taken with the Advanced Camera for Surveys (ACS) on board the *Hubble Space Telescope* (*HST*) and by 3.6, 4.5, 5.8, and 8.0 μm data taken with the Infrared Array Camera (IRAC; Fazio et al. 2004) on board *Spitzer*.

A catalog of $K_s < 21.5$ (Vega) sources has been selected in the GOODS/EIS CDFS. Photometric redshifts based on up to eight broad bands ($BVI_{775}z_{850}JK_s$ and IRAC 3.6 and 4.5 μm bands) have been obtained for the whole sample, using the publicly available multiwavelength data and the public code HYPERZ (Bolzonella et al. 2000) with the GISSEL98 spectral energy distribution (SED) template library (Bruzual & Charlot 1993). Dust corrections have been taken into account through the convolution of the SED templates with the Calzetti et al. (2000) reddening law.

Although *U*-band data exist for the CDFS, they have not been included in the input catalogs for the photometric redshift algorithms, as the *U*-band images have shallower depth and poorer resolution than the ACS and ISAAC images in the same field. However, *U*-band images have been used to control the HYPERZ output: for every K_s-band source with a counterpart in the shallow *U*-band catalogs, the resulting photometric redshift was determined as the best-fit value constrained to a maximum redshift $z_{phot} = 2$, as higher redshift sources are unlikely to be bright at such short wavelengths. In addition, the public code BPZ (Benítez 2000) has been used to obtain a second independent set of redshift estimates for all the $K_s < 21.5$ sources. In the cases of sources with HYPERZ photometric redshifts $z_{phot} > 2$ not confirmed by BPZ, we adopted the lower estimates from the BPZ code. In addition, public COMBO17 photometric redshifts (Wolf et al. 2004) have been used to replace the redshift estimates of those sources with magnitude $R < 23.5$ (Vega) and $z < 1$ (the most accurate regime for COMBO17 redshifts). Further details on the redshift estimations for the total $K_s < 21.5$ sample are given in a separate paper (Caputi et al. 2006). Figure 1*a* compares the obtained photometric redshifts with spectroscopic redshifts for all those $K_s < 21.5$ sources in the GOODS/EIS CDFS included in different publicly available spectroscopy samples (e.g., Vanzella et al. 2005; Le Fèvre et al. 2004). We observe a very good agreement between the photometric estimates and the real redshifts in most cases, with a median for the absolute relative errors of $|dz| = |z_{spec} - z_{phot}|/(1 + z_{spec}) = 0.02$. Figure 1*b* shows the corresponding histogram of relative errors.

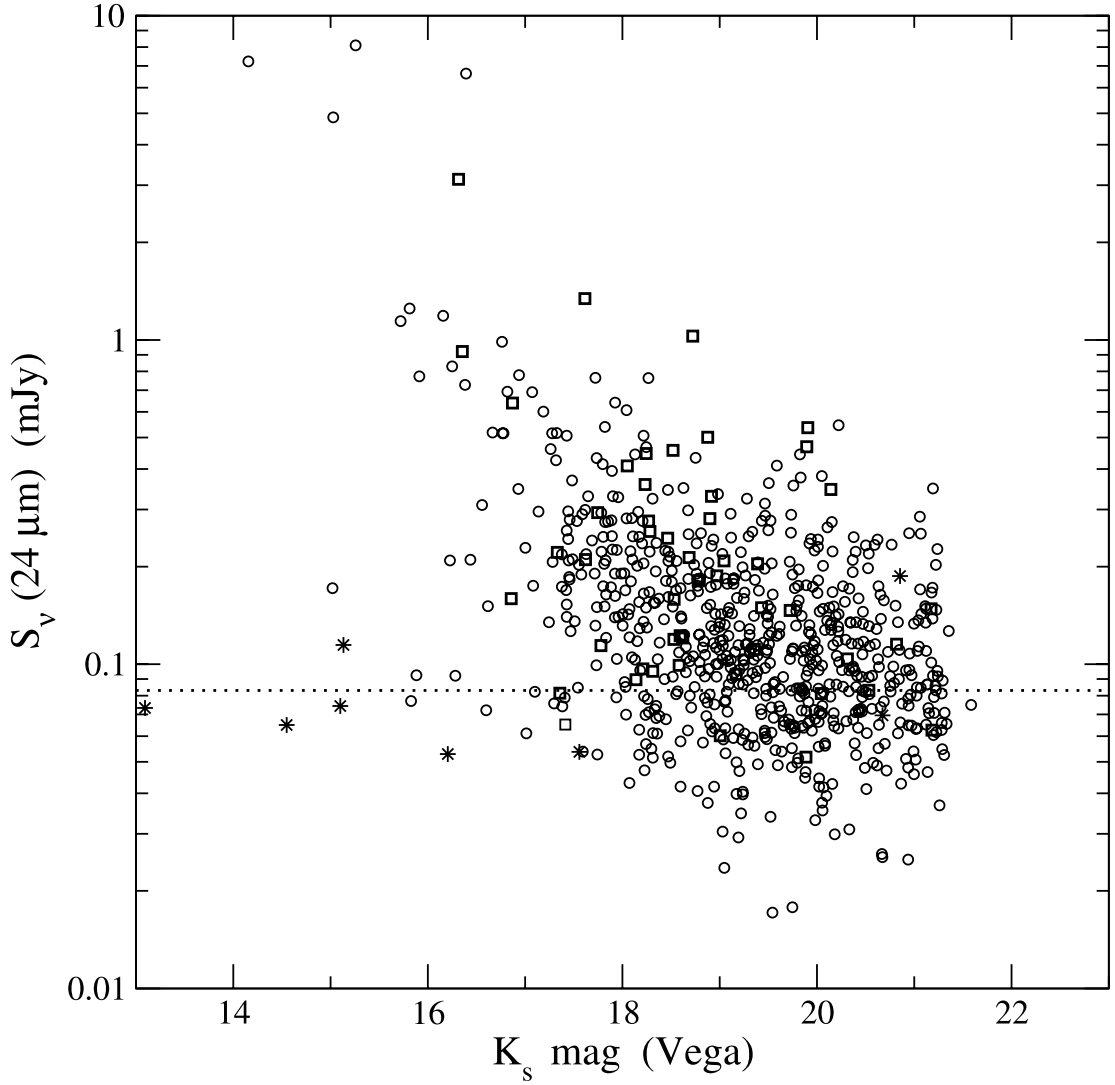


FIG. 2.—Plot of 24 μm fluxes vs. K_s magnitudes for the MIPS 24 μm sources in the GOODS/CDFS associated with a $K_s < 21.5$ counterpart. The circles, squares, and asterisks correspond to normal galaxies, active galaxies, and Galactic stars, respectively. The dotted line indicates the limit of ~80% completeness of the 24 μm catalog, above which the K_s-band identification is ~94%.

The rms of the distribution is 0.03. However, in spite of the good accuracy obtained for the photometric redshifts, the incorporation of available spectroscopic redshifts is of much benefit for any study of a galaxy redshift distribution. Thus, in order to maximize the quality of the final redshift catalog, the existing spectroscopic redshifts in the CDFS have been used to replace the photometric estimates of the $K_s < 21.5$ sources whenever possible (i.e., 23% of the total $K_s < 21.5$ sample).

2.2. *Cross-Correlation of the Catalogs*

We cross-correlated the $K_s < 21.5$ GOODS/CDFS source catalog with the *Spitzer* MIPS 24 μm GTO/CDFS catalog both to investigate and put constraints on the mid-IR emission of K_s-selected galaxies and to identify and characterize the optical/near-IR properties of the *Spitzer* MIPS 24 μm sources in the GOODS South field. This work presents the results of the latter, while a full analysis of 24 μm detected and nondetected K_s-selected galaxies in the GOODS/CDFS will be presented elsewhere (K. I. Caputi et al. 2006, in preparation). In addition, the IRAC and MIPS properties of galaxies selected with colors $J-K_s > 2.3$ are studied by Papovich et al. (2006).

We looked for 24 μm counterparts of the $K_s < 21.5$ selected sources in the GOODS/CDFS using a matching radius of 2″ to minimize the number of multiple identifications. The astrometric accuracy of the MIPS 24 μm images (e.g., Le Floc'h et al. 2005) allows the use of such a small matching distance. We found 812 $K_s < 21.5$ selected sources associated with MIPS 24 μm sources within this radius. In 65/812 cases, we found two or more K_s-selected sources associated with the same 24 μm source. In these cases we selected the closest counterpart, leaving 747 24 μm sources with a $K_s < 21.5$ identification. We identified a negligible fraction (11/747) of Galactic stars among these MIPS 24 μm sources, and we exclude them from all the following analysis. We determined redshifts for each of the remaining 736 24 μm sources; 36% of them have spectroscopic redshifts, and 21% more have COMBO17 photometric redshifts. The remaining 43% have HYPERZ/BPZ photometric redshifts; 521/747 sources are above the 24 μm catalog 80% completeness limit—i.e., they have $S_\nu > 83$ μJy. On the other hand, we find four K_s-selected objects that could be associated with two or more 24 μm sources. All of these cases correspond to low-redshift galaxies, with spectroscopic redshifts $z_{\rm spec} < 0.13$. Individual inspection

TABLE 1
COMPLETENESS LIMITS FOR THE K_s-BAND IDENTIFICATIONS OF THE *Spitzer* MIPS 24 μm SOURCES IN THE GOODS/CDFS

24 μm Flux S_ν (μJy)	K_s-Band Identification Completeness (%)
>250	100
>200	99
>150	96
>100	95
>83	94

of both the K_s and 24 μm images suggests the *Spitzer* MIPS detection of multiple nodes of mid-IR emission for each of these nearby galaxies. In Figure 2, we show the total 24 μm flux S_ν versus K_s magnitude for the 747 MIPS sources with $K_s < 21.5$ identifications in the GOODS/CDFS. In the four cases of multiple MIPS sources associated with a single K_s-band object, we considered that the 24 μm flux was the sum of the different 24 μm components; 686/747 MIPS 24 μm sources in the GOODS/CDFS have counterparts classified as normal galaxies (circles in Fig. 2), while 50/747 are active ones (active galactic nuclei [AGNs] or quasi-stellar objects [QSOs]; squares in Fig. 2). The identification of K_s sources with active galaxies is based on the cross-correlation with the X-ray catalogs available for the CDFS (Szokoly et al. 2004). This approach provides only a lower limit to the fraction of active galaxies among the 24 μm galaxy population (Alonso-Herrero et al. 2006; Donley et al. 2005). The cross-correlations of the $K_s < 21.5$ GOODS/CDFS source catalog with the *Spitzer* MIPS 24 μm GTO/CDFS catalog allows us to achieve a completeness limit of $\sim$94% for the identification of MIPS 24 μm sources with flux $S_\nu > 83$ μJy in the GOODS/CDFS (see Table 1).

As we mentioned above, our HYPERZ photometric redshift determinations are based on the SED fitting of the galaxies made using the templates in the GISSEL98 library of Bruzual & Charlot (1993). Also, this SED fitting procedure has been used to determine derived parameters (e.g., estimated stellar mass) for all the galaxies, independent of whether the redshifts were from HYPERZ/BPZ, COMBO17, or spectroscopic. The GISSEL98 library is composed of a wide range of synthetic SEDs based on stellar spectra but does not have any optical to near-IR power-law SED. To investigate the impact of this limitation in our redshift distribution of MIPS 24 μm galaxies, we identified the presence of 24 μm power-law SED galaxies in the GOODS/CDFS using the catalog of IR power-law sources constructed by Alonso-Herrero et al. (2006). We found 20 24 μm galaxies with IR power-law spectra in the GOODS/CDFS. Nine of these power-law galaxies have spectroscopic redshifts, leaving only 11 power-law sources with a HYPERZ/BPZ photometric redshift (and 7/11 are X-ray–detected; see § 4). Consequently, plausible erroneous redshift estimates due to inadequate SED template fitting are reduced to a very minor fraction of the 24 μm sources studied here, and thus they should have a basically negligible impact on all the analysis in this work.

2.3. *Summary of Properties of the 24 μm Source Sample Analyzed in This Work*

For clarity, we summarize the properties of the source sample analyzed in this work as follows:

1. Our sample is composed of the 747 24 μm sources in $\sim$131 arcmin^2 of the GOODS/CDFS that have a $K_s < 21.5$ (Vega) counterpart; 521/747 sources have a flux above the GTO catalog 80% completeness limit, i.e., $S_\nu(24\ \mu\text{m}) > 83$ μJy. These 521 objects constitute $\sim$94% of all the MIPS 24 μm sources with $S_\nu(24\ \mu\text{m}) > 83$ μJy in the GOODS/CDFS.

2. Only 11/747 sources in our sample are identified as galactic stars; 50/747 sources are X-ray–classified AGNs or QSOs. The remaining 686/747 sources are normal galaxies (i.e., no X-ray AGN or QSO).

3. We determined redshifts for each of the 736 galaxies in our sample (i.e., all sources except the 11 galactic stars); 36% of these redshifts are spectroscopic, and 21% additional redshifts have been taken from the COMBO17 photometric redshift catalog (only for sources with R-band magnitude $R < 23.5$, Vega, and redshifts $z < 1$). The photometric redshifts for the remaining 43% of the sample have been obtained using HYPERZ/BPZ and are based on broadband photometry covering from the optical B band through the 4.5 μm band.

In this way, our sample allows us to identify and characterize the evolution down to faint fluxes for most of the sources composing the 24 μm background.

Pérez-González et al. (2005) have carried out a study of MIPS 24 μm detections using a different photometric redshift technique. Their approach uses empirical SEDs rather than synthetic templates, and it can fit redshifts using a wider range of multiwavelength data. Their work has the advantage of having been applied to larger fields. However, high signal-to-noise ratio data may not be available in all bands for these large areas, and thus their resulting redshifts have a typical accuracy of about 10%, significantly worse than those obtained here. Our approach depends on high-quality and homogeneous input data, only available for very limited areas of the sky. By combining the results of both works, it is possible to (1) determine overall trends and the effects of cosmic variance based on the approach of Pérez-González et al. (2005) and (2) prove the redshift distribution more accurately in a more limited sky region based on the approach in this paper.

3. THE REDSHIFT DISTRIBUTION OF 24 μm GALAXIES IN THE GOODS/CDFS

Figure 3*a* shows the redshift distribution of the MIPS 24 μm galaxies with $K_s < 21.5$ counterparts in the GOODS/CDFS. The empty (shaded) histogram corresponds to all ($S_\nu > 83$ μJy) sources. The peaks in the redshift distribution at $z \sim 0.7$ and 1.1 are due to the effect of large-scale structure in the CDFS (e.g., Le Fèvre et al. 2004). We find that 72% of the 24 μm galaxies lie at redshifts $z < 1.5$, while the remaining 28% are found to be at $z \geq 1.5$ (the percentages are similar for the samples containing all and only $S_\nu > 83$ μJy galaxies). This confirms the existence of a substantial population of mid-IR sources at high redshifts. Approximately half of the $z \geq 1.5$ sources have the characteristic colors of extremely red galaxies (ERGs), $(I_{775} - K_s) > 4.0$ (Vega), indicating that an important fraction of the high-redshift mid-IR background is constituted by optically obscured sources, as possibly expected (see Yan et al. 2004).

Figure 3*b* shows the normalized redshift distributions of the MIPS 24 μm galaxies with $K_s < 21.5$ counterparts (*black dashed and solid lines*, for all and $S_\nu > 83$ μJy sources, respectively), compared to the redshift distribution of the total $K_s < 21.5$ galaxy population (*gray solid line*) in the same field. Several features are present in all the three curves, which are the consequence of cosmic variance effects. In contrast, we observe the presence of a depression in the redshift distribution of 24 μm galaxies at redshift $z \sim 1.5$ and a bump at redshift $z \sim 1.9$, both of which do not appear in the total $K_s < 21.5$ galaxy curve.

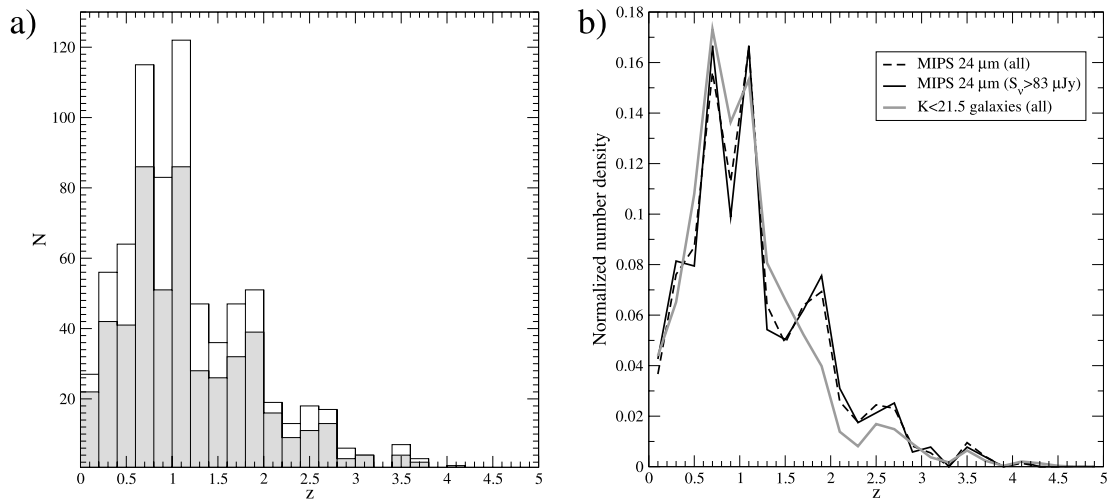


FIG. 3.—(*a*) Redshift distribution of the MIPS 24 μm galaxies with $K_s < 21.5$ counterparts in the GOODS/CDFS: all sources and sources with $S_\nu > 83$ μJy (*empty and shaded histograms*, respectively). (*b*) Normalized redshift distributions of all and $S_\nu > 83$ μJy 24 μm galaxies (*black dashed and solid lines*, respectively), compared to the normalized redshift distribution of the total $K_s < 21.5$ sample in the same field (*gray solid line*).

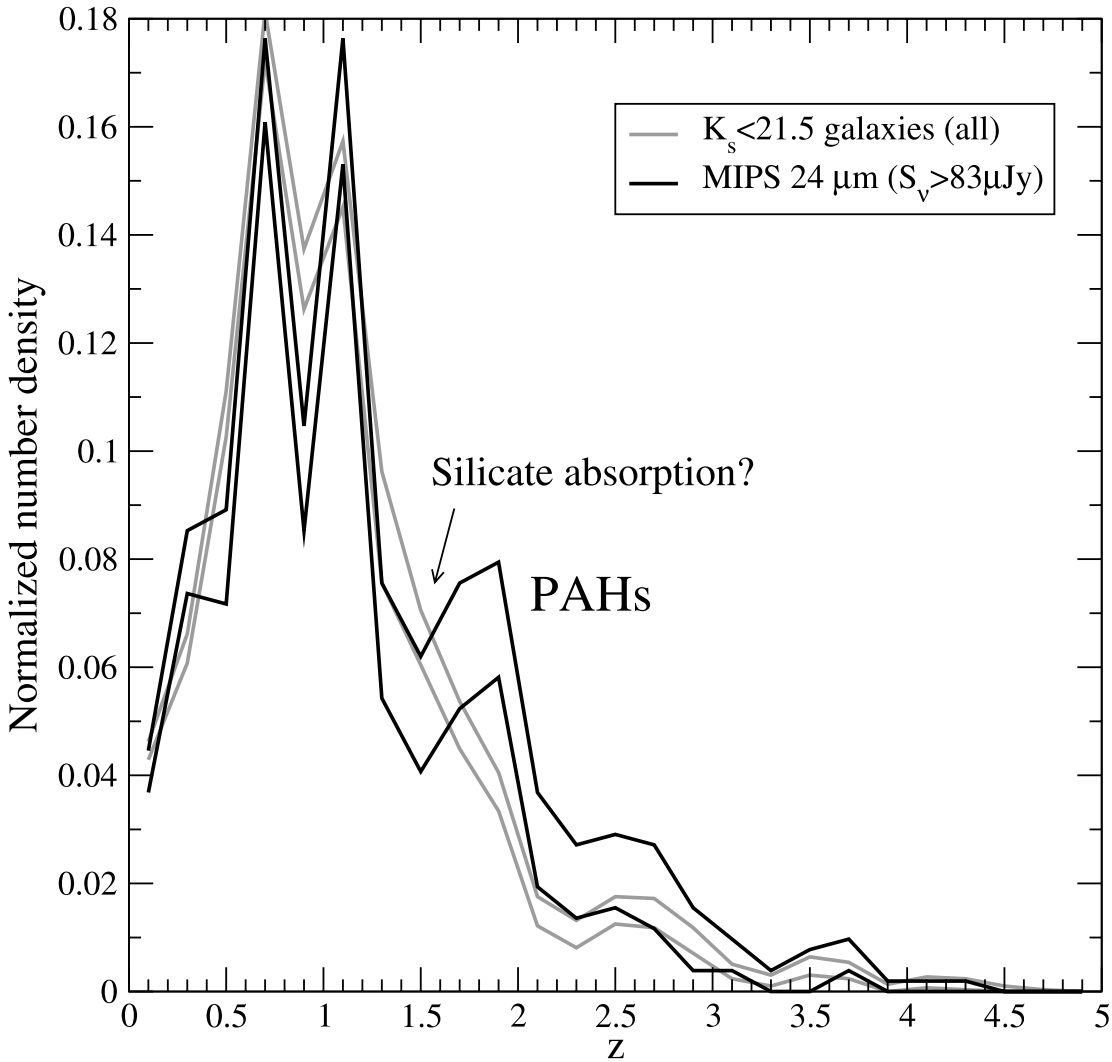


FIG. 4.—Plot of the 95% confidence limits on the normalized redshift distributions of the MIPS $S_\nu(24\ \mu\text{m}) > 83$ μJy galaxies (*black lines*) and all the $K_s < 21.5$ galaxies (*gray lines*). The bump in the redshift distribution of 24 μm galaxies at $z \sim 1.9$ indicates the presence of PAH emission at these high redshifts. The marginally significant depression at redshift $z \sim 1.5$ might be due to silicate absorption.

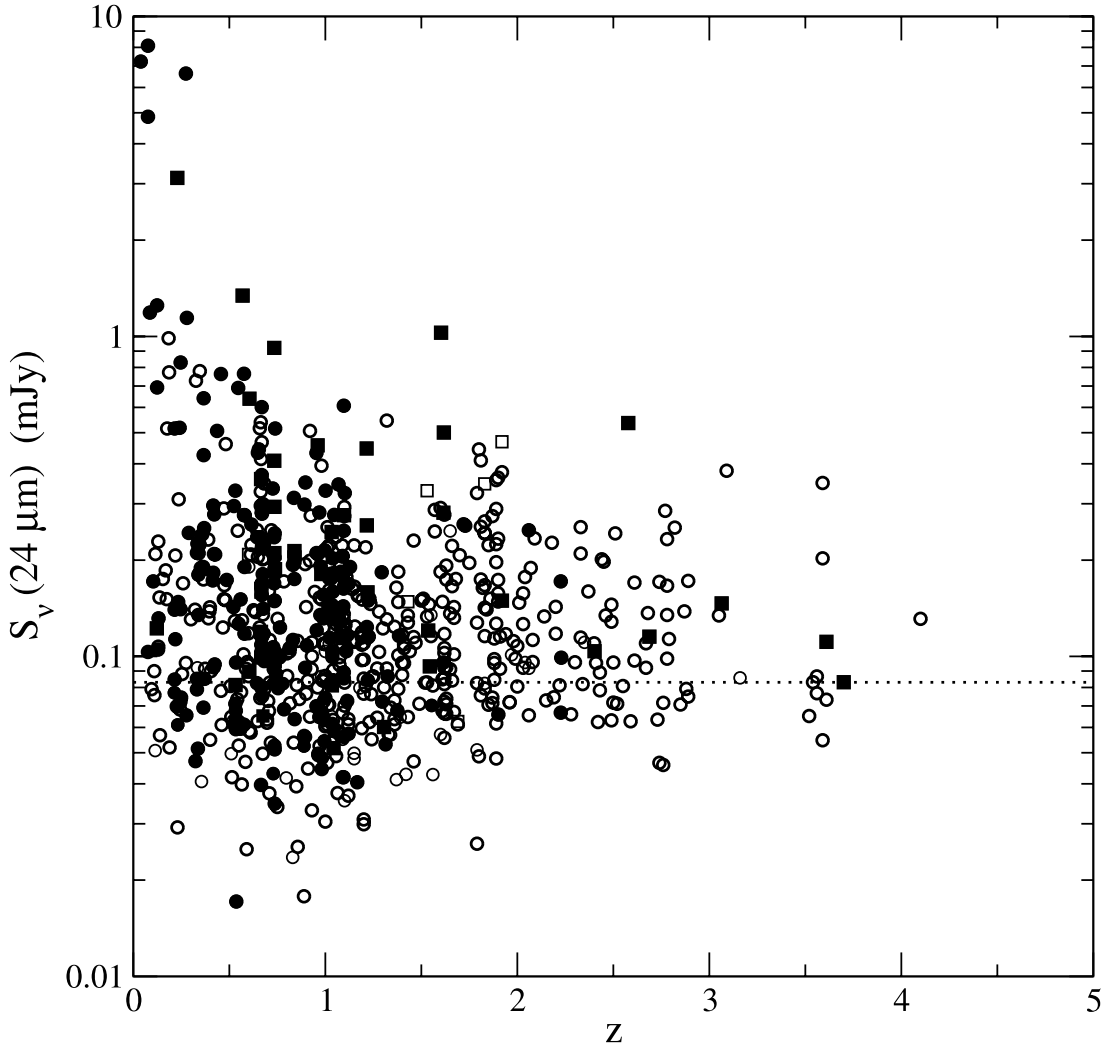


FIG. 5.—Plot of 24 μm flux vs. redshift for the MIPS 24 μm galaxies in the GOODS/CDFS associated with a $K_s < 21.5$ counterpart. The symbols are the same as in Fig. 2. Filled symbols indicate spectroscopic redshifts.

To assess the significance of the features observed exclusively on the 24 μm galaxy redshift distributions, we computed confidence limits on the different curves. We performed Monte Carlo simulations to create 1000 mock redshift catalogs, alternatively for the total $K_s < 21.5$ galaxy population and for the MIPS 24 μm galaxies with flux $S_\nu > 83$ μJy. We constructed each mock catalog assigning to each source a random redshift, with a Gaussian probability centered at the original redshift z of the source and a dispersion equal to $0.02\,(1 + z)$ (i.e., the median error at the corresponding redshift). The redshifts of those sources with spectroscopic values were left fixed. We recomputed the normalized redshift distribution for each mock catalog and determined confidence limits on the original distribution curves. The 95% confidence limits on the total $K_s < 21.5$ galaxy and the MIPS ($S_\nu > 83$ μJy) galaxy distributions are shown in Figure 4.

Figure 4 shows that, even taking into account the error bars, the peak in the 24 μm redshift distribution at $z \sim 1.9$ is significant, lying ~ 4 σ from the original total $K_s < 21.5$ galaxy curve. Thus, we conclude that the redshift distribution of 24 μm galaxies presents a real secondary bump at these high redshifts. This secondary peak has been predicted by Lagache et al. (2004) and is the consequence of the selection effect produced by the presence of PAH emission features entering the observed 24 μm band. Given the width of the 24 μm filter (whose transmission covers the wavelength range $\sim$20–28 μm), both the 7.7 and the 8.6 μm PAH lines could contribute to the redshift distribution peak observed at $z \sim 1.9$. Our results allow us to conclude that PAH molecules must be already present in star-forming galaxies at high redshifts.

The confidence limits shown in Figure 4 also indicate that the depression observed in the 24 μm redshift distribution at $z \sim 1.5$ is only marginally significant within our sample. The existence of such a depression could be interpreted as due to the 9.8 μm silicate absorption feature entering the 24 μm filter at this redshift, which has been observed for some galaxies in previous works (Houck et al. 2005; Yan et al. 2005). However, given the errors in the redshift distributions presented here, we cannot reach any firm conclusion on the possible selection effect produced by silicate absorption at high redshifts.

We also see a substantial deficit of 24 μm sources at redshift $z \sim 0.9$, with respect to the total $K_s < 21.5$ sources. At this redshift, a positive selection effect on 24 μm galaxies would be expected due to the presence of the 12.7 μm PAH emission line. The observed relative deficit of bright mid-IR selected galaxies indicates that, within our sample, star-forming galaxies are present in a minor proportion at this redshift. This is quite likely due to a mere cosmic variance effect. However, we note that this deficit in our 24 μm sample occurs at the same redshift where

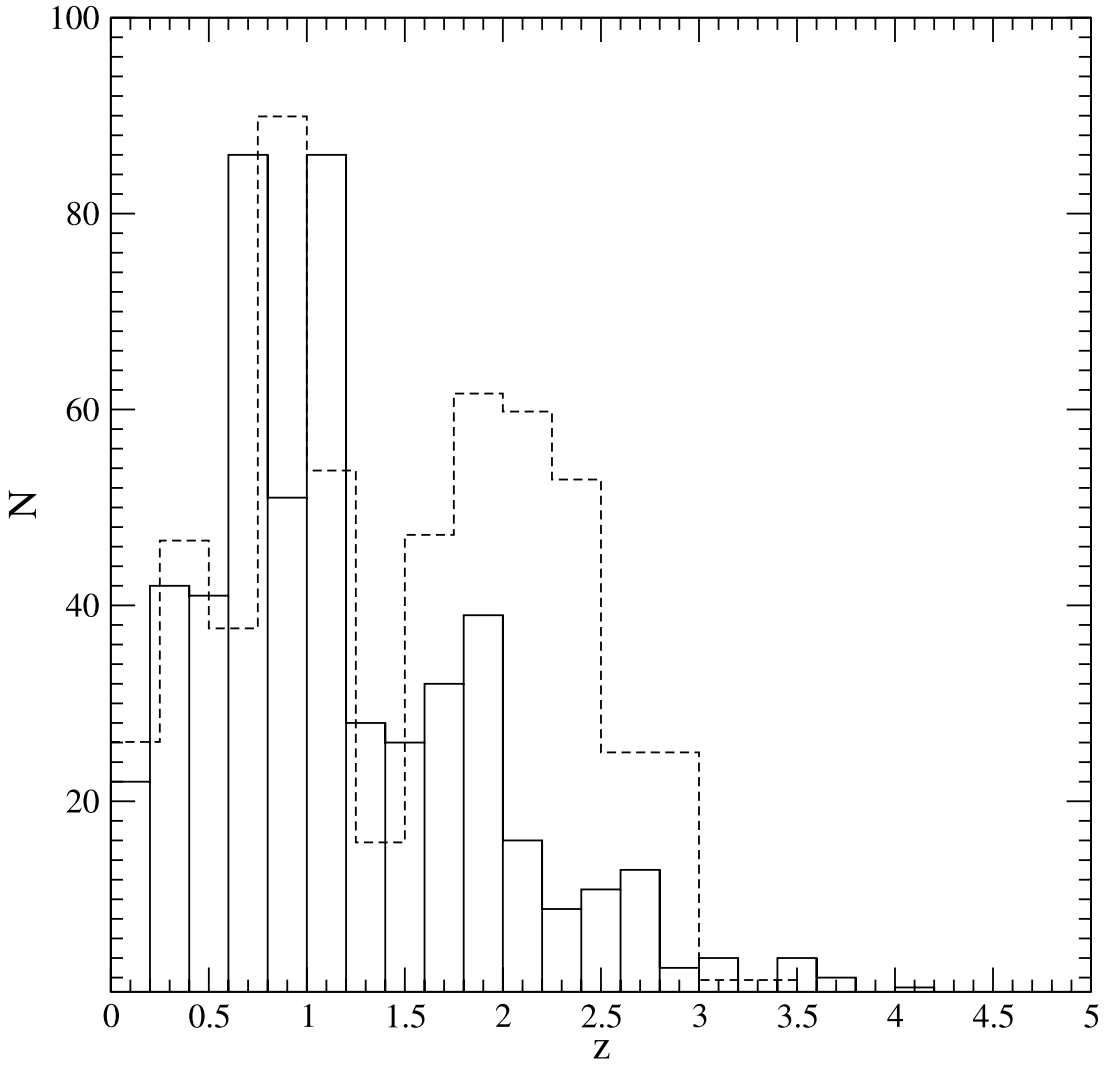


FIG. 6.—Comparison of the observed redshift distribution of MIPS 24 μm galaxies in the GOODS/CDFS (*solid histogram*) with the redshift distribution predicted by Lagache et al. (2004; *dashed histogram*). Both distributions correspond to sources with flux $S_\nu(24\ \mu\text{m}) > 83\ \mu$Jy in an area of 131 arcmin^2.

there is a dip in the total $K_s < 21.5$ redshift distribution. If we consider that galaxy interactions are a triggering mechanism for star formation, then it will be possible that star formation activity is particularly inhibited in regions with an underdensity of objects. The study of similar regions in other areas of the sky is necessary to determine whether the two facts are actually related.

Evidence of the existence of PAH emission in the spectra of a few high-redshift $1.7-1.8 < z < 2.6-2.8$ galaxies has recently been presented by Houck et al. (2005), Yan et al. (2005), and Lutz et al. (2005). In this work, we extend this evidence through the study of the redshift distribution of the whole 24 μm galaxy population. It is interesting to note, however, that both Houck et al. (2005) and Yan et al. (2005) found that only a minority of their galaxies at $z \sim 1.7-2.8$ showed clear PAH emission features in their spectra, while most of their remaining high-redshift galaxies were AGN-dominated or had silicate absorption features. The difference in the nature of the sources dominating Houck et al. and Yan et al. samples can be explained taking into account that their objects are, on average, an order of magnitude more luminous than most of the sources analyzed in this work. Deep 24 μm samples are necessary to uncover a substantial population of PAH galaxies at redshift $z \sim 2$. Figure 5 shows the 24 μm flux of each galaxy S_ν versus redshift z. The symbols are the same as in Figure 2. Filled symbols correspond to sources with spectroscopic redshifts. Within our sample, we see that only a few bright $S_\nu(24\ \mu\text{m}) > 0.5$ mJy sources are placed at high redshift ($z \gtrsim 1.5$) and that they are all active galaxies. At fainter fluxes $S_\nu \lesssim 0.3$ mJy, starbursts produce the bulk of the mid-IR emission at high redshifts.

Pérez-González et al. (2005) found that 24% of the 24 μm galaxies with $S_\nu > 83\ \mu$Jy in an extended region of the CDFS and the Hubble Deep Field–North (HDFN) were at redshifts $z > 1.5$, in agreement with our value of 28% within the errors and taking into account the different fields surveyed. However, their redshift distribution does not show the PAH-induced peak at $1.6 \lesssim z \lesssim 2.2$. They suggested that this feature may have been blurred by the errors in photometric redshifts; this suggestion is confirmed by our detection of the PAH bump using redshifts of higher accuracy. Taken together, the two studies show that the drop in the number of sources beyond $z \sim 1.2$ holds generally and is not just observed in the CDFS. In addition, we show that there is a significant peak produced by PAH emission on top of this general trend.

Figure 6 shows the comparison of our observed redshift distribution of 24 μm galaxies in the GOODS/CDFS (*solid*

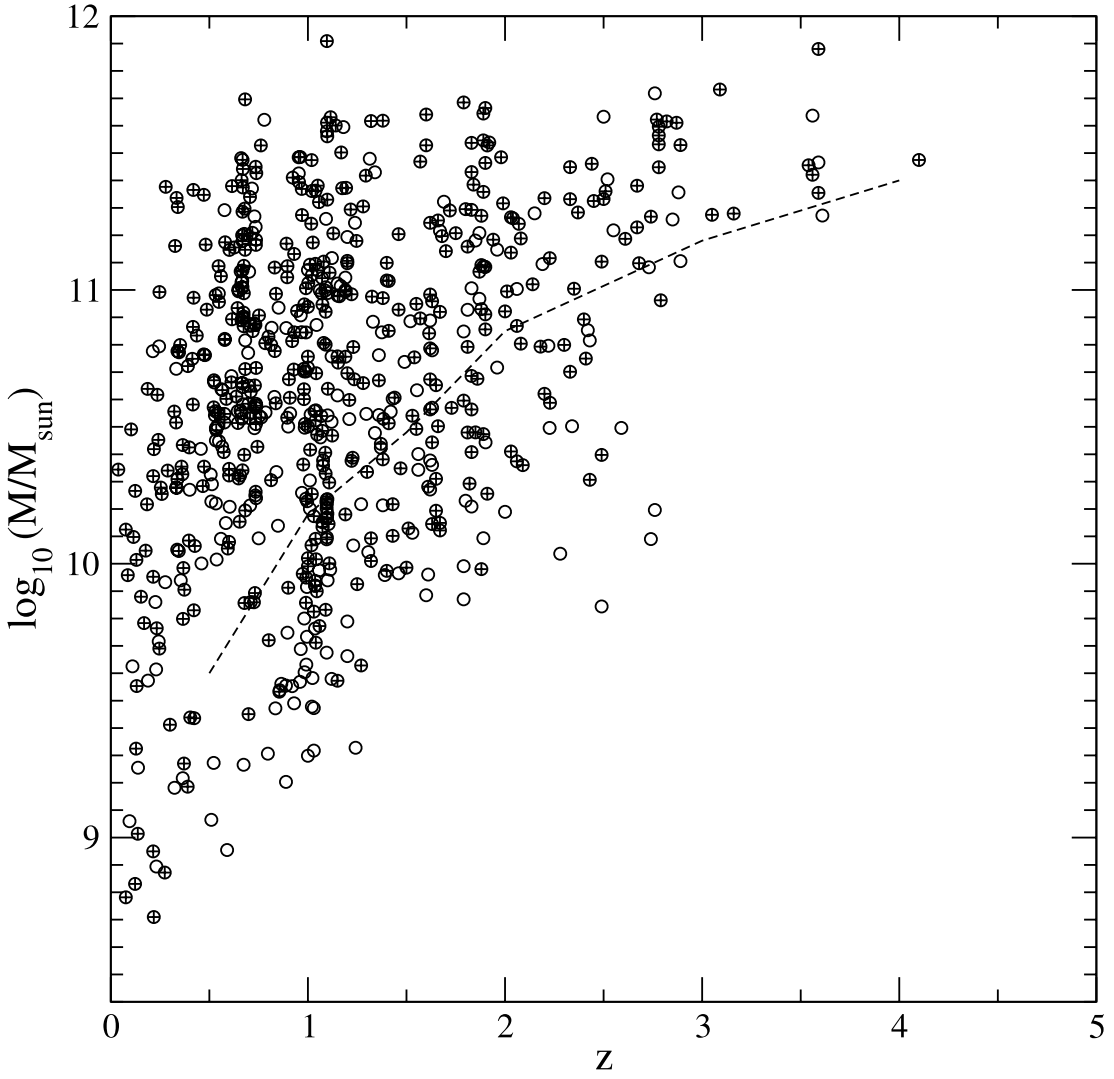


FIG. 7.—Estimated assembled stellar masses for the MIPS 24 μm galaxies with $K_s < 21.5$ counterparts in the GOODS/CDFS. The symbols with a plus sign correspond to galaxies with flux $S_\nu(24\ \mu\text{m}) > 83\ \mu$Jy. The dashed line indicates the estimated mass completeness limits imposed by the $K_s < 21.5$ survey. However, we note that these limits are basically irrelevant for the galaxies with flux $S_\nu(24\ \mu\text{m}) > 83\ \mu$Jy, as the K_s-band identification completeness for these galaxies is ~94%.

histogram) with the distribution predicted by Lagache et al. (2004) using the Lagache et al. (2003) model (*dashed histogram*). Both distributions correspond to sources with flux $S_\nu > 83\ \mu$Jy in an area of 131 arcmin^2. The observed and predicted distributions have 521 and 518 galaxies, respectively, confirming that the Lagache et al. (2003) model reproduces the observed number counts very well. Also in agreement with the model, we find that a significant population of 24 μm galaxies lie at redshifts $z > 1.5$, and our accurate redshift determinations reveal the predicted secondary peak in the redshift distribution at $z \sim 1.9$ produced by the presence of PAH emission. However, the fraction of galaxies at redshifts $z > 1.5$ is significantly overpredicted by the Lagache et al. model. Other models (e.g., Chary & Elbaz 2001) basically predict a negligible fraction of sources at redshifts $z > 1.5$ and also do not fit the observed redshift distribution. Therefore, theoretical models require further refinements to reproduce the distant infrared-emitting galaxy populations.

4. THE ASSEMBLED STELLAR MASSES OF MIPS 24 μm GALAXIES

Figure 7 shows the estimated assembled stellar masses of the MIPS 24 μm galaxies versus redshift z in the GOODS/CDFS. The estimation of the stellar masses is based on the optical–to–near-IR SED fit of each galaxy at the determined redshift (either spectroscopic, from COMBO17, or HYPERZ/BPZ) and is completely independent of its 24 μm properties. We determined estimated stellar masses for all the 24 μm galaxies with a $K_s < 21.5$ identification, except for any X-ray–classified AGN/QSO or any other X-ray source without a suitable GISSEL98 template optical–to–near-IR SED fit. We excluded the latter objects to avoid galaxies with partial contamination of the optical–to–near-IR light by a hidden AGN. The stellar masses are computed from the modeled rest-frame K_s-band galaxy luminosity of each galaxy, where the mass-to-light ratios have a minimum dependence on the SED star formation histories or dust corrections (see Caputi et al. [2005, 2006] for further details). The resulting stellar mass estimates are typically accurate within a factor of $\lesssim 2$. A single power-law Salpeter initial mass function (IMF) over stellar masses $M = 0.1$–$100\ M_\odot$ has been assumed throughout. The estimated mass completeness limits for counterparts of the MIPS 24 μm galaxies are 1.5×10^{10}, 7.0×10^{10}, and $1.5 \times 10^{11}\ M_\odot$ at redshifts $z = 1, 2$, and 3, respectively, based on the $K_s = 21.5$ mag limit and the median of the k-corrections. However, it should be noted that the mass completeness limits are basically

irrelevant for the sources with flux $S_\nu > 83$ μJy (symbols with plus signs in Fig. 7), as the K_s-band identifications are almost complete above this limit.

Inspection of Figure 7 shows that, at least at redshifts $z \lesssim 1$, star formation activity takes place in galaxies of a wide range of assembled stellar masses, from $\sim 10^9$ to $\sim 10^{12}$ $M_\odot$. At high redshifts $z \gtrsim 2.5$, the existence of a significant population of massive $M > 10^{11}$ $M_\odot$ star-forming galaxies is revealed in the mid-IR at the depth of the GTO/CDFS images. It is now commonly believed that a fraction of present-day massive galaxies is already in place at high redshifts (Cimatti et al. 2004; Glazebrook et al. 2004; Caputi et al. 2005, 2006). However, it is still unclear when the bulk of the stars in these massive galaxies was formed (see Papovich et al. 2006). The identification of massive objects on the MIPS 24 μm images can put constraints on their star formation histories and the amount of stellar mass built up at different redshifts.

5. CONSTRAINTS ON THE STAR FORMATION HISTORY

5.1. *The Evolution of Star-forming Galaxies with Redshift*

The study of the physical properties of IR-selected galaxies at different redshifts is of importance to understand how star formation evolved with cosmic time. In this section, we use the 24 μm fluxes of the galaxies in the GOODS/CDFS in conjunction with the redshift and stellar mass estimations, to study the evolution of star formation activity.

Chary & Elbaz (2001) and Elbaz et al. (2002) showed that the mid-IR luminosities of nearby galaxies were correlated (with some scatter) with their bolometric IR luminosity $L_{\rm IR}$, defined as $L_{\rm IR} = L(8{-}1000\ \mu{\rm m})$. They fitted the following set of relations:

$$L_{\rm IR} = 11.1^{+5.5}_{-3.7}\,[\nu L_\nu(15\ \mu{\rm m})]^{0.998}, \quad (1)$$

$$= 0.89^{+0.38}_{-0.27}\,[\nu L_\nu(12\ \mu{\rm m})]^{1.094}, \quad (2)$$

$$= 4.78^{+2.37}_{-1.59}\,[\nu L_\nu(6.75\ \mu{\rm m})]^{0.998} \quad (3)$$

$$\text{for } \nu L_\nu(6.75\ \mu{\rm m}) < 5\times 10^9\ L_\odot,$$

$$= 4.37^{+2.35}_{-2.13}\times 10^{-6}\,[\nu L_\nu(6.75\ \mu{\rm m})]^{1.62} \quad (4)$$

$$\text{for } \nu L_\nu(6.75\ \mu{\rm m}) \geq 5\times 10^9\ L_\odot,$$

where all the luminosities are in solar units. There are many indications that the overall SEDs of high-redshift infrared galaxies are similar to the local ones captured in equations (1)–(4). For example, the local far-IR/radio and mid-IR/radio correlations (Condon 1992) still hold at higher redshifts (Appleton et al. 2004). Composite SEDs of high-redshift infrared galaxies resemble local templates (e.g., Egami et al. 2004). The MIPS observations in the CDFS indicate that, at least to $z \sim 1$, galaxies have 24 and 70 μm flux ratios that follow the local distribution as a function of total IR luminosity. In addition, number count models assuming similar behavior can fit the 24, 70, and 160 μm data simultaneously (Lagache et al. 2004).

We used the 24 μm fluxes of the MIPS galaxies with a $K_s < 21.5$ counterpart in the GOODS/CDFS to compute their bolometric luminosities $L_{\rm IR}$, assuming the Chary & Elbaz (2001) relations in equations (1)–(4). We excluded all the known AGNs/QSOs from the present analysis. We considered that the 24 μm flux mapped the rest-frame 15, 12, and 6.75 μm fluxes in the redshift ranges $0.4 \leq z < 0.8$, $0.8 \leq z < 1.2$, and $2.0 \leq z < 3.0$, respectively. In the redshift range $1.2 \leq z < 2.0$, we assumed that the infrared luminosity $L_{\rm IR}$ was given by the average of the luminosities obtained using equations (2) and (3)–(4). Figure 8 shows the bolometric IR luminosities of the 24 μm galaxies versus assembled stellar mass in different redshift bins. The dotted lines delimit the region of luminosity completeness at the mean redshift of each bin, taking into account the $S_\nu(24\ \mu{\rm m}) = 83$ μJy limit and the fact that our K_s-band identifications are almost complete above that flux (i.e., the mass completeness limits imposed by the $K_s = 21.5$ cut are basically irrelevant above that limit).

Although for clarity the error bars are not shown in Figure 8, we estimated the errors on our computed bolometric luminosities using an independent set of models. We integrated the different Dale et al. (2001) and Dale & Helou (2002) SED templates, normalized to our observed 24 μm fluxes, to obtain the corresponding IR luminosities as a function of redshift. The complete set of the Dale et al. SEDs consists of 64 templates, each one characterized by a parameter α ($0.0625 < \alpha < 4.0$), which depends on the combination of the observed local SEDs used to construct these models. Compared to the values obtained with the Dale et al. templates, our luminosities based on the Chary & Elbaz (2001) formulae appear to be accurate within a factor of 2–3 to redshift $z \approx 1.5$. Above that redshift, the consideration of the complete set of the Dale et al. SEDs would yield uncertainties of up to a factor of 10–20 (Dale et al. 2005). However, Dale et al. (2005) recently used the Dale et al. templates to fit the observed 1–850 μm photometry of a sample of 75 local galaxies. The majority of these galaxies ($\gtrsim$75%) were best-fitted by templates with $2.0 < \alpha < 4.0$. As we explained above, there are many indications that the overall SEDs of high-redshift IR galaxies are similar to the local ones. Thus, this subset of the Dale et al. templates should be representative of the majority of the IR galaxy types also at high redshifts. If we restrict the comparison of our luminosities computed with the Chary & Elbaz formulae to those values obtained with the Dale et al. $2.0 < \alpha < 4.0$ templates, we find that the error bars would still be within a factor of 2–3 up to redshift $z \approx 2$, and a factor of 5 would be sufficient to account for the errors above that redshift. These factors should be representative of the error bars on the IR luminosities of the majority of our galaxies, including the errors introduced by the k-corrections within each of the considered redshift bins.

We observe that the evolution of the IR luminosities with redshift is still very significant, even taking into account the error bars. Figure 8*a* shows that most of the 24 μm galaxies at redshifts $0.4 \leq z < 0.8$ have infrared luminosities $L_{\rm IR} < 10^{11}$ $L_\odot$. The maximum observed infrared luminosities increase with redshift, and luminous infrared galaxies (LIRGs) characterized by 10^{11} $L_\odot < L_{\rm IR} < 10^{12}$ $L_\odot$ (Sanders & Mirabel 1996) are the dominant 24 μm sources at redshifts $0.8 \leq z < 1.2$ at the depth of the CDFS MIPS/GTO images (Le Floc'h et al. 2005). The majority of the mid-IR sources at $0.4 \leq z < 1.2$ are hosted by intermediate-mass galaxies with stellar masses 10^{10} $M_\odot \lesssim M \lesssim 10^{11}$ $M_\odot$, in agreement with recent findings by Hammer et al. (2005), although some more massive galaxies could also be classified as LIRGs at these redshifts. Within our surveyed area, there is virtually no ultraluminous infrared galaxy (ULIRG) with $L_{\rm IR} > 10^{12}$ $L_\odot$ at $z < 1.2$. ULIRGs might be present at these low redshifts, but are indeed very rare (e.g., Flores et al. 1999). At $1.2 \leq z \leq 2.0$, ULIRGs start to be a very significant population ($\sim$65% at $S_\nu > 83$ μJy), and they are also hosted by intermediate- to high-mass galaxies. At $z > 2$, the limits of the 24 μm survey only allow us to explore the bright IR luminosity end of the star formation activity. We observe sources with extremely high infrared luminosities 10^{12} $L_\odot < L_{\rm IR} < 10^{14}$ $L_\odot$, mainly harbored by galaxies with stellar masses $M > 10^{11}$ $M_\odot$. Our results on luminosity and SFR evolution agree well with

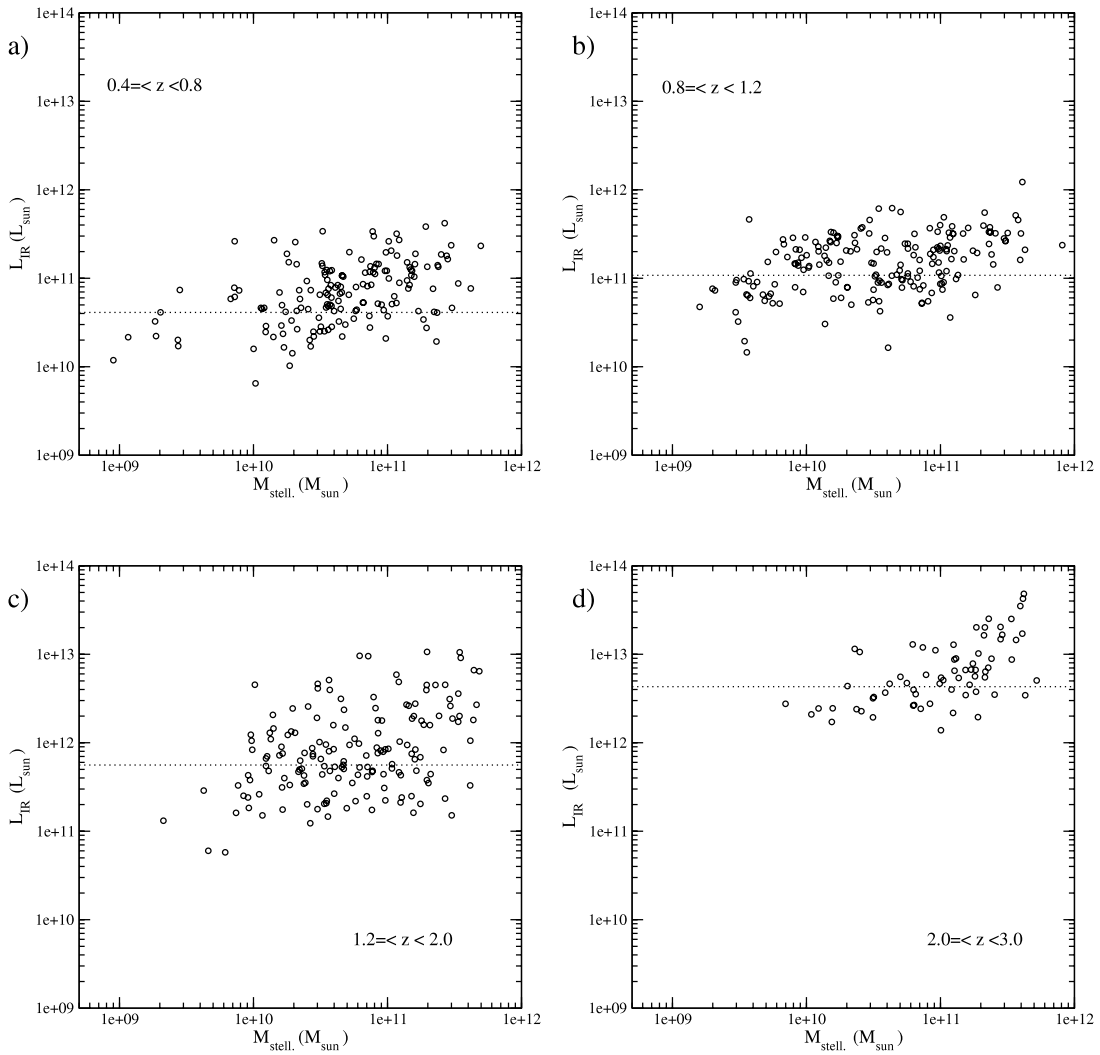


FIG. 8.—Bolometric infrared luminosities vs. assembled stellar masses for the MIPS 24 μm galaxies with $K_s < 21.5$ counterparts in the GOODS/CDFS, in different redshift bins: (*a*) $0.4 \leq z < 0.8$, (*b*) $0.8 \leq z < 1.2$, (*c*) $1.2 \leq z < 2.0$, and (*d*) $2.0 \leq z < 3.0$. The dotted lines delimit the region of completeness at the mean redshift of each bin, taking into account the $S_\nu(24\ \mu\text{m}) = 83\ \mu$Jy limit and the fact that our K_s-band identifications are almost complete above that flux (i.e., the mass completeness limits imposed by the $K_s = 21.5$ cut are basically irrelevant above that limit).

the studies for larger fields made by Le Floc'h et al. (2005) and Pérez-González et al. (2005).

Thus, Figure 8 confirms the global trend of a high degree of evolution in the star formation activity from low to high redshifts. The extremely high IR luminosities observed at $z \gtrsim 2$ show that star formation has been a much more violent process in the past, and these violent episodes of star formation must have built up a significant part of the stellar mass content of at least a fraction of present-day massive galaxies. We explore in more detail this possibility in § 5.2, where we analyze and constrain the typical timescales for star formation of galaxies with different assembled stellar masses at different redshifts.

5.2. *Probing Star Formation in Different Mass Galaxies*

An estimator of the instantaneous SFR of a galaxy based on its bolometric infrared luminosity has been obtained by Kennicutt (1998):

$$\text{SFR} = 1.72 \times 10^{-10} L_{\text{IR}}, \qquad (5)$$

where the SFR is given in units of solar masses per year, the luminosity L_{IR} is in solar units, and a Salpeter IMF over stellar masses $M = 0.1\text{–}100\ M_\odot$ is assumed. We used equation (5) to obtain an estimate of the instantaneous SFR in the 24 μm galaxies studied here and to explore the relation of this SFR with the already assembled stellar mass of each galaxy, at different redshifts.

Figure 9 shows the evolution of the SFR with redshift for galaxies with assembled stellar masses in different mass bins. In all the panels, the dashed line delimits the region of completeness of the observed SFR versus redshift, as imposed by the flux limit $S_\nu(24\ \mu\text{m}) = 83\ \mu$Jy. We find that the IR-derived SFR grows exponentially with redshift, independent of the galaxy stellar mass (of course, the lower envelope of SFR is a consequence of the limits of the 24 μm survey, but the maximum observed values do exponentially grow with redshift). However, Figure 9*a* shows that, at a given redshift, most of the lowest mass galaxies have relatively small SFRs, which are at most marginally above the completeness limit of the 24 μm survey analyzed here. This effect is particularly evident at high redshifts $z \gtrsim 2$, where we observe a lack of galaxies with stellar mass $M < 1.5 \times 10^{10}\ M_\odot$ and SFR above the completeness limit. Unless the minor fraction of unidentified sources with $S_\nu(24\ \mu\text{m}) > 83\ \mu$Jy constitutes a biased population of low-mass galaxies at high redshifts, we conclude

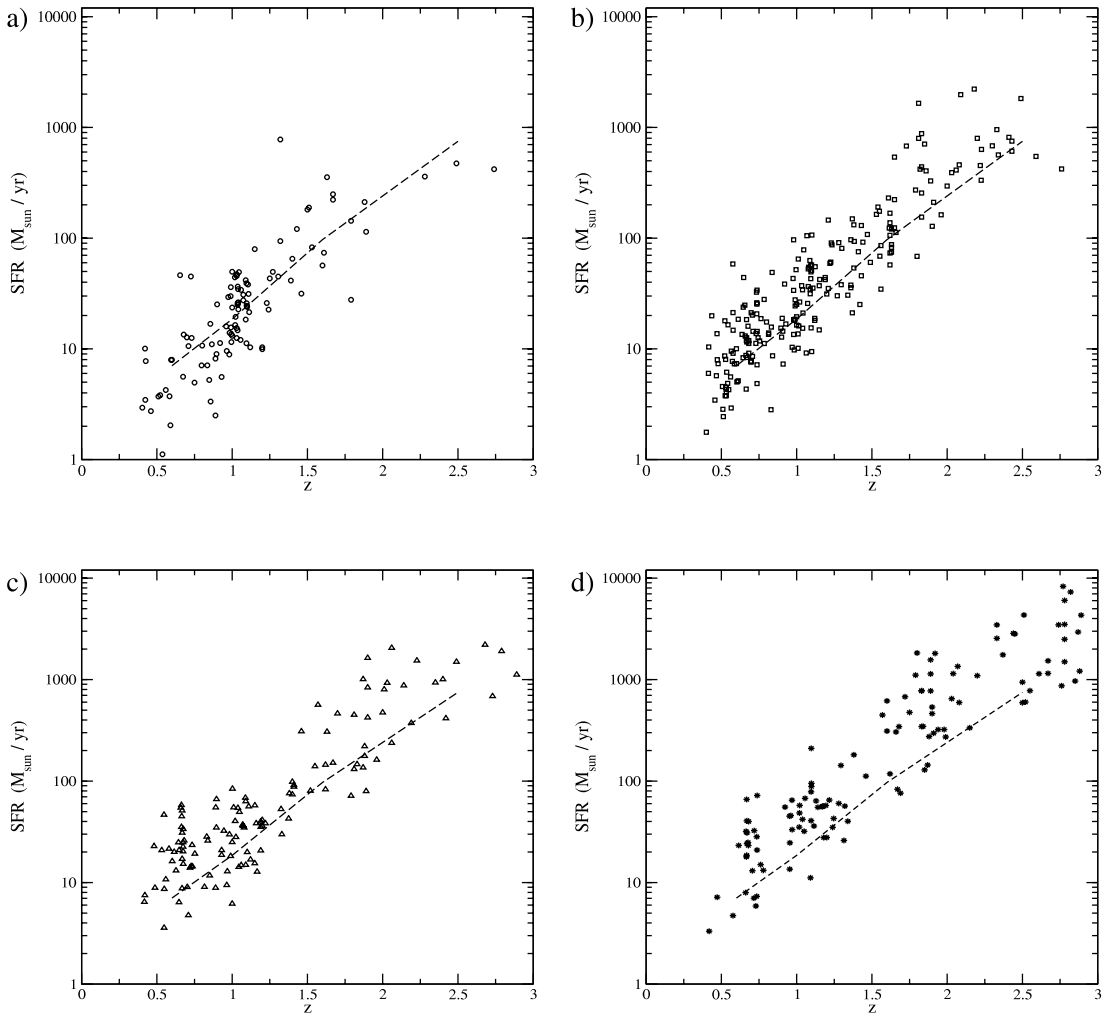


FIG. 9.—Evolution of the SFR of galaxies with different assembled stellar mass: (*a*) $M < 1.5 \times 10^{10}\ M_{\odot}$, (*b*) $1.5 \times 10^{10}\ M_{\odot} \leq M < 7.0 \times 10^{10}\ M_{\odot}$, (*c*) $7.0 \times 10^{10}\ M_{\odot} \leq M < 1.5 \times 10^{11}\ M_{\odot}$, and (*d*) $M \geq 1.5 \times 10^{11}\ M_{\odot}$. In all the panels, the dashed line delimits the region of completeness of the observed SFRs as imposed by the flux limit $S_{\nu}(24\ \mu\text{m}) = 83\ \mu\text{Jy}$.

that low-mass objects with very high SFR (SFR $\gtrsim 500\ M_{\odot}\ \text{yr}^{-1}$) are indeed rare at $z \gtrsim 2$. On the contrary, galaxies with greater stellar mass $M \geq 1.5 \times 10^{10}\ M_{\odot}$ and SFR $\gtrsim 500\ M_{\odot}\ \text{yr}^{-1}$ are progressively found at higher redshifts.

Figure 10 shows the ratio of already assembled stellar mass over the instantaneous SFR, M/SFR, versus redshift z for the 24 μm galaxies with a $K_s < 21.5$ counterpart in the GOODS/CDFS. Different symbols correspond to galaxies with stellar masses in different mass ranges, as in Figure 9. The solid line shows the age of the universe as a function of redshift, while the dashed line indicates the upper limit of the typical lifetime of a starburst ($\sim$0.1 Gyr). The assembled stellar masses have been computed as in § 4 and are completely independent of the 24 μm properties of each galaxy. If the SFRs in a galaxy were larger in the past or at most stayed constant over cosmic time, the ratio M/SFR would give an upper limit for the lifetime of the source. Therefore, Figure 10 allows putting constraints on the star formation history of the MIPS 24 μm galaxies present at different redshifts.

A first striking conclusion is that, at high redshifts $z \sim 2$–3, a starburst lifetime appears to be sufficient to construct a substantial fraction and up to the whole amount of the stellar mass of some massive galaxies. If equations (1)–(5) are still applicable at those redshifts, very high SFRs are predicted, ranging from $\sim$500 to 5000 $M_{\odot}\ \text{yr}^{-1}$. In this way, a stellar mass of $\approx 10^{10}$–$10^{11}\ M_{\odot}$ could be constructed in a $\sim$0.01–0.1 Gyr period of time. However, this does not necessarily mean that all these systems are being formed at $z \sim 2$–3. Recent works suggest that a non-negligible fraction of present-day massive galaxies would be present before even higher ($z \gtrsim 3$) redshifts (van Dokkum et al. 2004; Caputi et al. 2004, 2005, 2006). Certainly, we find other 24 μm massive galaxies for which the derived lifetimes M/SFR are larger (up to $\sim$1 Gyr), indicating that these galaxies would be present since higher redshifts, and that star formation histories longer than a single burst lifetime are necessary to build the stellar mass present in them. Moreover, other massive galaxies with SFRs below the limits of the 24 μm survey analyzed here also exist at redshift $z \sim 2$–3 (K. I. Caputi et al. 2006, in preparation).

It is interesting to note that the best-fit optical to near-IR SEDs for our 24 μm galaxies at redshifts $z \gtrsim 2$ correspond to different galaxy ages, many of which exceed the maximum $\sim$1 Gyr lifetime derived with the ratio M/SFR. This fact could indicate that the instantaneous SFRs derived from the 24 μm fluxes of these galaxies were not constant or larger in the past. In order for these galaxies to have ages of $\sim$1–3 Gyr (as those derived from the best-fit SEDs), their SFRs must have been *smaller* at some moment in the past. This strongly suggests that some massive

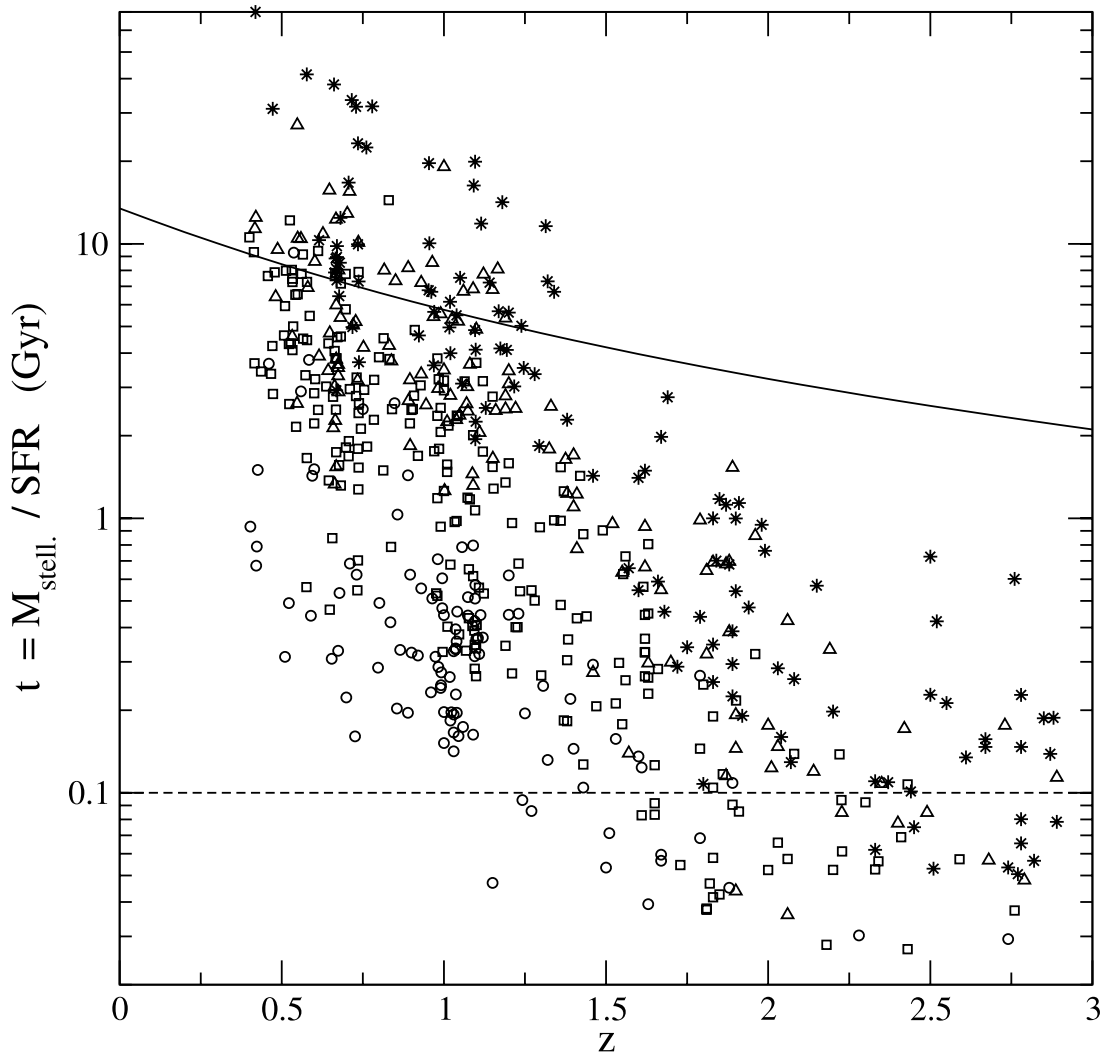


FIG. 10.—Ratio between the assembled stellar mass and the instantaneous SFR of MIPS 24 μm galaxies with $K_s < 21.5$ counterparts in the GOODS/CDFS vs. redshift. Different symbols indicate different assembled stellar mass ranges: $M < 1.5 \times 10^{10}\ M_\odot$ (*circles*), $1.5 \times 10^{10}\ M_\odot \leq M < 7.0 \times 10^{10}\ M_\odot$ (*squares*), $7.0 \times 10^{10}\ M_\odot \leq M < 1.5 \times 10^{11}\ M_\odot$ (*triangles*), and $M \geq 1.5 \times 10^{11}\ M_\odot$ (*asterisks*). The solid line shows the age of the universe as a function of redshift, while the dashed line indicates an upper limit to the typical lifetime of a starburst (0.1 Gyr).

galaxies could already be in place at higher redshifts and experience a noncontinuous star formation history, with temporary episodes of high star formation activity (see also Papovich et al. 2005). Those suffering such episodes at $z \sim 2$–3 would be detected as hyperluminous infrared galaxies at these redshifts in mid-IR surveys. If this is the case, the major episodes of star formation at $z \sim 2$–3 would not account for the complete assembly history of these massive galaxies. A similar argument has been given by Hammer et al. (2005), who proposed that the stellar mass growth of intermediate-mass galaxies at $z < 1$ could proceed by successive star formation episodes characterized by a LIRG phase.

As mentioned in § 3, a substantial fraction of the 24 μm sources at high redshifts have the characteristic colors of ERGs, $(I_{775} - K_s) > 4.0$ (Vega). Based on the best-fit optical to near-IR SEDs, the large majority of the ERGs have been formed in short timescales (instantaneously or with characteristic times $\tau \leq 1$ Gyr). For many of them, the best-fit age is larger than the SED-derived time formation scale, i.e., age >1 Gyr. However, even when these characteristics would correspond to systems undergoing passive evolution, the SED of most of these ERGs can only be properly fitted with considerable amounts of dust extinction. We find that the median of the color excess in the 24 μm ERGs at $z > 2$ is $E(B - V) \approx 0.30$, a value too high to conclude that these galaxies could be passive systems even from the optical to near-IR point of view.

It should be emphasized that the SFRs computed here assume that the mid-IR sources are purely star-forming. Another possibility is that at least part of the mid-IR emission of these sources is due to the presence of an AGN, in which case the real SFR would be lower than our estimated values. We note, however, that even when, e.g., only one-half of the mid-IR luminosities of the $z \sim 2$–3 galaxies analyzed here were due to star formation, the derived SFR would still be sufficiently high so as to construct stellar masses of the order of $\gtrsim 10^{10}\ M_\odot$ in a burst timescale. The properties of these high-redshift massive mid-IR galaxies resemble those of submillimeter galaxies, whose redshift distribution has a median of $z = 2.2$–2.4 (Chapman et al. 2003, 2005). Thus, it is expected that the 24 μm galaxy population at the depth of the GTO images contains at least a fraction of the submillimeter galaxy population (see Egami et al. 2004; Ivison et al. 2004).

At lower redshifts $z \lesssim 1$, the completeness limits of the samples allow us to determine that star formation spans a wide

range of timescales, in agreement with results obtained from the analysis of *ISO* sources (Franceschini et al. 2003). Moreover, we find that these timescales for star formation activity depend on galaxy mass, with more massive star-forming galaxies probably experiencing more prolonged star formation histories. In particular, for the high-mass end $M \geq 1.5 \times 10^{11}\ M_{\odot}$ at $z \lesssim 1$, we see that the derived timescales are larger than the age of the universe at the corresponding redshifts. This fact indicates that the SFR of these galaxies was not constant over time, but larger in the past. This plausible differential star formation history for star-forming galaxies of different assembled stellar masses at $z \lesssim 1.0$ is in agreement with recent results reported in the literature (Heavens et al. 2004).

Although the derived timescales M/SFR for massive ($M \geq 1.5 \times 10^{11}\ M_{\odot}$) galaxies at $z \lesssim 1$ indicate prolonged star formation histories, different possibilities exist for the way in which star formation proceeded through cosmic time. Star formation could have proceeded quiescently, i.e., with relatively small SFR sustained through long (>0.1 Gyr) periods of time. Alternatively, as discussed earlier, star formation might have been noncontinuous, with the production of multiple burstlike episodes. Both ways—or also some combination of the two—could have lead to the construction of the stellar mass contained in these massive galaxies. However, the number densities of both all and $S_{\nu}(24\ \mu\mathrm{m}) > 83\ \mu$Jy massive galaxies at $z \sim 3$ is only ~20% of the corresponding number densities at $z < 1$ (Caputi et al. 2006; K. I. Caputi et al. 2006, in preparation). Thus, the major episodes of star formation activity produced at very high redshifts could be responsible for the construction of stellar mass in at most a minor fraction of the massive 24 μm galaxies observed at $z < 1$. Also, it is likely that most of the massive galaxies undergoing high star formation activity at $z \sim 2$–3 do not have significant amounts of remaining gas to condense into stars by redshift $z \sim 1$. Thus, massive 24 μm galaxies at $z \sim 2$–3 are probably not the progenitors of the massive 24 μm galaxies at $z \sim 1$. The star formation history of massive IR galaxies at low redshifts should have mainly proceeded by some combination of quiescent activity and relatively modest burstlike episodes.

It is interesting to analyze the evolution with redshift of the efficiency of the burstlike star formation mode to construct a significant fraction of a galaxy stellar mass. As stated above, at redshifts $z \sim 2$–3, the typical starburst lifetime of 0.01–0.1 Gyr is sufficient to form a substantial fraction of the stellar mass of some massive galaxies ($M \geq 1.5 \times 10^{11}\ M_{\odot}$). At redshifts $z \sim 1$–2, only low- to intermediate-mass galaxies ($M \leq 7.0 \times 10^{10}\ M_{\odot}$) could form in a burst lifetime. Within the limits of our sample and the volume surveyed, no galaxy appears to be able to have built up in a burst timescale at $z \lesssim 1$. This does not mean that the burstlike mode cannot proceed in different mass galaxies at these low redshifts, but that each individual burst would only be sufficient to construct an additional minor amount of the galaxy-assembled stellar mass (i.e., SFR/M would be low). Thus, our results suggest that the potential importance of the burstlike mode of formation shifts from high- to low-mass galaxies with decreasing redshift (note, however, that we cannot completely probe star formation in galaxies with stellar mass $M \lesssim 10^{11}\ M_{\odot}$ at $z \sim 2$–3). In fact, each individual burstlike episode can play only a secondary role in galaxy building at $z \lesssim 1$ (see also Papovich et al. 2005).

6. DISCUSSION AND SUMMARY

In this work, we present K_s-band identifications of the MIPS 24 μm galaxies in the GOODS/CDFS at the depth of the *Spitzer*/GTO surveys [with ~94% of identification completeness for sources with flux $S_{\nu}(24\ \mu\mathrm{m}) > 83\ \mu$Jy]. A $K_s < 21.5$ (Vega) galaxy survey is sufficient for this purpose. The remaining nonidentified galaxies are mostly faint mid- and near-IR sources. A minor fraction (7%) of the 747 identified objects correspond to X-ray–selected active galaxies. Active galaxies are among the brightest 24 μm sources at high redshifts (see Houck et al. 2005).

MIPS 24 μm galaxies in the GOODS/CDFS span the redshift range $z = 0$–4, and 28% of the population lies at redshifts $z \gtrsim 1.5$ at the depth of the GTO data. This confirms the predictions of a substantial population of mid-IR–selected galaxies at high redshifts. We determined the existence of a significant bump in the redshift distribution of 24 μm galaxies at $z \sim 1.9$, in agreement with predictions made by Lagache et al. (2004) using the Lagache et al. (2003) model. This secondary peak in the redshift distribution of 24 μm galaxies indicates the existence of PAH spectral features in $z \sim 1.9$ star-forming galaxies. We also observed the predicted depression in the redshift distribution at $z \sim 1.5$, although with marginal significance, which could be driven by silicate absorption. However, the overall observed redshift distribution differs significantly from the distribution predicted by the Lagache et al. (2003) and other models, indicating that revisions are required to understand the high-redshift infrared-luminous galaxy population.

The mid-IR galaxy population is mainly composed of normal star-forming galaxies at redshifts $0.4 \leq z < 0.8$, while LIRGs start to be dominant at $0.8 \leq z < 1.2$. We derived estimated assembled stellar masses of 10^9–$10^{12}\ M_{\odot}$ for the 24 μm galaxies at $z \lesssim 1.2$. Massive star-forming galaxies appear to dominate the mid-IR output progressively at higher redshifts. A considerable fraction of the stellar mass density of the universe is contained in bright 24 μm sources: galaxies with flux $S_{\nu}(24\ \mu\mathrm{m}) > 83\ \mu$Jy contain ~35% of the stellar mass density at redshifts $z = 0.5$–1.5 and ~40% of the stellar mass density at $z \sim 1.5$–3.0. This corresponds to ~30%, 15%, 10%, and a minimum of 5% of the local value at redshifts $z \approx 0.75$, 1.25, 1.75, and 2.5, respectively (K. I. Caputi et al. 2006, in preparation). Thus, we conclude that bright 24 μm galaxies have a significant role in the history of stellar mass assembly.

We find that, at redshifts $z \lesssim 1.2$, the IR-derived timescales for star formation activity increase with the already assembled galaxy mass. Mid-IR galaxies with intermediate to high assembled stellar masses ($M \gtrsim 10^{10}\ M_{\odot}$) appear to be suffering rather prolonged star formation histories, while lower mass ($M \lesssim 10^{10}\ M_{\odot}$) galaxies, on the contrary, are characterized by star formation activity on shorter timescales. At higher redshifts $z \gtrsim 2$, massive galaxies are dominant, and all the derived timescales for the $S_{\nu}(24\ \mu\mathrm{m}) > 83\ \mu$Jy sources are $\lesssim$1 Gyr. Star formation history at high redshifts is likely to have proceeded in a series of burstlike episodes and, in a substantial fraction of massive galaxies, a single burst lifetime (0.01–0.1 Gyr) is sufficient to assemble a stellar mass of $\approx 10^{10}$–$10^{11}\ M_{\odot}$. We conclude, then, that the burstlike mode was probably an efficient way to construct the bulk of the stellar mass of massive galaxies at high redshifts.

At $z \sim 1$–2, on the contrary, the burstlike mode can be effective only for the formation of galaxies with mass $M \lesssim 7.0 \times 10^{10}\ M_{\odot}$, and individual bursts can play only a secondary role in galaxy building by redshifts $z \lesssim 1$. Recently, Bell et al. (2005) found that the majority of the 24 μm galaxies present at redshift $z \sim 0.7$ in the CDFS have regular spiral morphologies rather than irregular or peculiar morphologies. In conjunction, Bell et al. morphological determinations and our results on the lack of galaxies built up in a burst at $z \lesssim 1$ suggest that morphology

could be linked to the mode of star formation activity (see also Papovich et al. 2005). Galaxies with no ongoing or mainly quiescent star formation would show regular shapes, while galaxies suffering important burstlike episodes of star formation activity would appear as irregular. To test this hypothesis, a detailed morphological study of 24 μm galaxies as a function of stellar mass and redshift would be necessary.

Results recently published in the literature suggest a "downsizing" history for the formation of the stellar mass, where star formation proceeds from high- to low-mass galaxies (Heavens et al. 2004; Juneau et al. 2005). Our conclusions support a similar downsizing mechanism for the efficiency of the burstlike mode. This fact also suggests that massive star-forming galaxies at high redshifts are not the progenitors of the massive star-forming galaxies found to be at $z \lesssim 1$, which are characterized by much longer star formation histories. The properties of 24 μm galaxies at $z \gtrsim 2$ suggest, on the contrary, a likely connection with submillimeter galaxies. Current interpretations of submillimeter galaxies indicate that this population could contain the progenitors of the most massive E/S0 galaxies present in the local universe (e.g., Stevens et al. 2003). The high SFR characterizing mid-IR–selected galaxies at $2 \lesssim z \lesssim 3$ suggests a similar conclusion for the high-redshift 24 μm galaxy population. However, some recent works suggest that a non-negligible fraction of present-day massive galaxies would be in place at even higher ($z \gtrsim 3$) redshifts, indicating that the determination of the first epoch of formation of massive spheroids is still to be discovered.

This paper is based on observations made with the *Spitzer* Observatory, which is operated by the Jet Propulsion Laboratory (JPL), California Institute of Technology, under NASA contract 1407. It is also based on observations made with the Advanced Camera for Surveys on board the *Hubble Space Telescope*, operated by NASA/ESA, and with the Infrared Spectrometer and Array Camera on the "Antu" Very Large Telescope, operated by the European Southern Observatory in Cerro Paranal, Chile, and that form part of the publicly available GOODS data sets. We thank the GOODS teams for providing reduced data products.

We thank the anonymous referee for his/her useful comments and suggestions that improved the discussion of results in this paper. Support for this work was provided by NASA through contract 960785, issued by JPL/Caltech. K. I. C. acknowledges CNES and CNRS funding. R. J. M. acknowledges the support of the Royal Society.

REFERENCES

Alonso-Herrero, A., et al. 2006, ApJ, in press (astro-ph/0511507)
Appleton, P. N., et al. 2004, ApJS, 154, 147
Bell, E. F., et al. 2005, ApJ, 625, 23
Benítez, N. 2000, ApJ, 536, 571
Bolzonella, M., Miralles, J.-M., & Pelló, R. 2000, A&A, 363, 476
Borys, C., Chapman, S., Halpern, M., & Scott, D. 2003, MNRAS, 344, 385
Bruzual, A. G., & Charlot, S. 1993, ApJ, 405, 538
Calzetti, D., Armus, L., Bohlin, R. C., Kinney, A. L., Koorneef, J., & Storchi-Bergmann, T. 2000, ApJ, 533, 682
Caputi, K. I., Dunlop, J. S., McLure, R. J., & Roche, N. D. 2004, MNRAS, 353, 30
———. 2005, MNRAS, 361, 607
Caputi, K. I., McLure, R. J., Dunlop, J. S., Cirasuolo, M., & Schael, A. M. 2006, MNRAS, in press (astro-ph/0511571)
Chapman, S. C., Blain, A. W., Ivison, R. J., & Smail, I. R. 2003, Nature, 422, 695
Chapman, S. C., Blain, A. W., Smail, I. R., & Ivison, R. J. 2005, ApJ, 622, 772
Chary, R., & Elbaz, D. 2001, ApJ, 556, 562
Cimatti, A., et al. 2004, Nature, 430, 184
Condon, J. J. 1992, ARA&A, 30, 575
Dale, D. A., & Helou, G. 2002, ApJ, 576, 159
Dale, D. A., Helou, G., Contursi, A., Silbermann, N. A., & Kolhatkar, S. 2001, ApJ, 549, 215
Dale, D. A., et al. 2005, ApJ, 633, 857
Désert, F.-X., Boulanger, F., & Puget, J.-L. 1990, A&A, 237, 215
Donley, J. L., Rieke, G. H., Rigby, J. R., & Pérez-González, P. G. 2005, ApJ, 634, 169
Egami, E., et al. 2004, ApJS, 154, 130
Elbaz, D., Cesarsky, C. J., Chanial, P., Aussel, H., Franceschini, A., Fadda, D., & Chary, R. R. 2002, A&A, 384, 848
Fazio, G. G., et al. 2004, ApJS, 154, 10
Flores, H., et al. 1999, ApJ, 517, 148
Franceschini, A., Aussel, H., Cesarsky, C. J., Elbaz, D., & Fadda, D. 2001, A&A, 378, 1
Franceschini, A., et al. 2003, A&A, 403, 501
Genzel, R., & Cesarsky, C. J. 2000, ARA&A, 38, 761
Giavalisco, M., et al. 2004, ApJ, 600, L93
Glazebrook, K., et al. 2004, Nature, 430, 181
Hammer, F., Flores, F., Elbaz, D., Zheng, X. Z., Liang, Y. C., & Cesarsky, C. 2005, A&A, 430, 115
Heavens, A., Panter, B., Jiménez, R., & Dunlop, J. 2004, Nature, 428, 625
Houck, J. R., et al. 2005, ApJ, 622, L105
Ivison, R. J., et al. 2004, ApJS, 154, 124
Juneau, S., et al. 2005, ApJ, 619, L135
Kennicutt, R. C., Jr. 1998, ApJ, 498, 541
Lagache, G., Dole, H., & Puget, J.-L. 2003, MNRAS, 338, 555
Lagache, G., et al. 2004, ApJS, 154, 112
Le Fèvre, O., et al. 2004, A&A, 428, 1043
Le Floc'h, E., et al. 2004, ApJS, 154, 170
———. 2005, ApJ, 632, 169
Lonsdale, C., et al. 2004, ApJS, 154, 54
Lutz, D., Valiante, E., Sturm, E., Genzel, R., Tacconi, L. J., Lehnert, M. D., Sternberg, A., & Baker, A. J. 2005, ApJ, 625, L83
Papovich, C., Dickinson, M., Giavalisco, M., Conselice, C. J., & Ferguson, H. C. 2005, ApJ, 631, 101
Papovich, C., et al. 2004, ApJS, 154, 70
———. 2006, ApJ, in press (astro-ph/0511289)
Pérez-González, P. G., et al. 2005, ApJ, 630, 82
Rieke, G. H., et al. 2004, ApJS, 154, 25
Sanders, D. B., & Mirabel, I. F. 1996, ARA&A, 34, 749
Scott, S. E., et al. 2002, MNRAS, 331, 817
Stevens, J. A., et al. 2003, Nature, 425, 264
Szokoly, G. P., et al. 2004, ApJS, 155, 271
van Dokkum, P. G., et al. 2004, ApJ, 611, 703
Vanzella, E., et al. 2005, A&A, 434, 53
Werner, M. W., et al. 2004, ApJS, 154, 1
Wolf, C., et al. 2004, A&A, 421, 913
Yan, L., et al. 2004, ApJS, 154, 75
———. 2005, ApJ, 628, 604